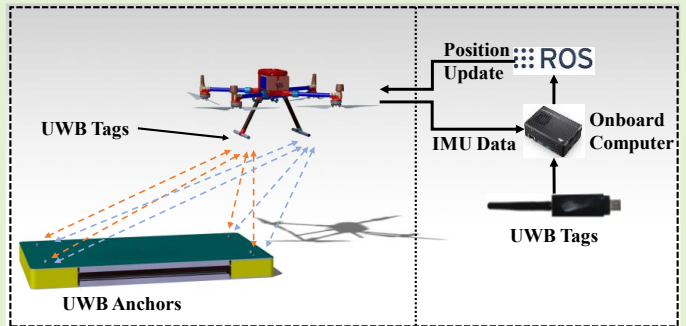


A UAV Localization System Based on Double UWB Tags and IMU for Landing Platform

Qingxi Zeng, Yu Jin, Haonan Yu, Xia You

Abstract—The successful landing of UAVs on unmanned vehicle landing platforms is critical for resolving the problem of insufficient range of UAVs in practical missions. Existing localization techniques for autonomous UAV landing are primarily vision-based, but this method is limited due to reliance on external lighting conditions. In this paper, we propose a localization system for UAV landing on a mobile platform, which can be conveniently deployed on an unmanned vehicle landing platform. Four UWB anchors were deployed on the 0.8m×1.4m rectangular unmanned vehicle landing platform. The spacing of the two tags installed on the UAV and the ranging information were used as constraints, and the linear least squares method was used to calculate the iterative initial coordinates of the gradient descent method to solve for the positions of the two UWB tags and fuse them with the IMU data to provide accurate coordinate for the safe landing of the UAV. By comparing the experiments with the linear least squares method in five experiments, it is demonstrated that the average RMSE of the localization system proposed in this paper is reduced by 61%.



Index Terms—IMU, Kalman filter, Landing, Localization, UAV, UWB.

I. INTRODUCTION

IN recent years, UAV technology has developed rapidly and is gradually being used in various fields such as aerial photography, aerial reconnaissance, geographic mapping, power line inspection, express delivery, agricultural plant protection, and environmental monitoring. However, due to the characteristics of UAVs, they still suffer from low load capacity and short range, and these drawbacks make it necessary to return to resupply points frequently and require specialized personnel to maneuver them during missions [1][2]. In contrast, unmanned vehicles have a high load capacity and can carry a large number of sensors, which makes such ground mobile platforms also have a good range. However, the apparent disadvantage of such ground mobile platforms is that their range of action is limited by the terrain [3].

Thus, UAVs and unmanned vehicles are highly complementary, and many researchers have combined them to control the landing of UAVs onto unmanned vehicles for

charging and replenishment [4-6]. Although UAVs can be maneuvered by professionals to land on unmanned vehicles, this solution is inefficient and prone to human error leading to the failure of UAVs landing on unmanned vehicles. Therefore, there is a need for UAVs to perform autonomous flights for landing onto an unmanned vehicle. UAV landing is one of the most dangerous aspects of UAV missions. When the UAV is flying autonomously for landing, it is crucial to obtain the real-time position of the UAV relative to the landing target area of the unmanned vehicle, and a few meters of localization error may lead to the failure of the UAV landing and crash.

Normally, it is widespread to use GPS for localization on UAVs, and it is widely believed that GPS has an error of 5 m or more under normal conditions [7]. Due to GPS error, UAVs cannot land accurately on the landing platform. RTK localization technology, with an error of centimeter level, can provide highly accurate position information to UAVs and make their land accurate on the landing platform. However, in many cases, RTK localization technology is not available, such as in urban canyons [8]. Therefore, researchers have proposed using vision-based methods for landing [9][10]. However, traditional vision-based localization techniques depend on external lighting conditions, such as at night or in the case of fire smoke, where vision-based localization systems are unavailable. Although some researchers have proposed using convolutional neural networks to detect cooperative marker centers and estimate cooperative marker directions in low-light environments, it has not been implemented on UAV platforms [11]. In addition, there is an approach that combines magnetic guidance with the vision to implement UAVs [12], but this approach is still very

Manuscript created August 10th, 2022. This work was supported by the Fundamental Research Funds for the Central Universities (Grant No. NJ2022019-5).

Qingxi Zeng, Yu Jin, and Haonan Yu are with the College of Automation Engineering, Nanjing University of Aeronautics and Astronautics, the Key Laboratory of Nuclear Technology Application and Radiation Protection in Astronautics (Nanjing University of Aeronautics and Astronautics), Ministry of Industry and Information Technology, and Nondestructive Detection and the Monitoring Technology for High Speed Transportation Facilities, Key Laboratory of Ministry of Industry and Information Technology, Nanjing, 211106 China (e-mail: autonavinuaa@163.com).

dependent on external light conditions.

Experiments with multiple UWB anchors deployment schemes were conducted in [13], which included the arrangement of four UWB anchors according to two schemes with poor localization geometry configurations. One scheme is to deploy the four UWB anchors on the four corners of a square with a side length of 2m. In the other UWB anchor deployment scheme, the four UWB anchors are deployed on the four corners of a cube with a side length of 0.6m. Compared with the former scheme, this scheme has a worse localization geometry configuration, and the experimental results show that the localization accuracy of the first UWB anchor deployment scheme is twice as high as that of the second UWB anchor deployment scheme, so [13] suggests to follow the first scheme for deployment. Although the error of the first scheme is smaller, the first scheme still has the problem of too large a deployment area for unmanned vehicles. In [14], UWB anchors were deployed near the landing area, and UWB was compared with RTK to determine whether the ultra-bandwidth real-time localization system could be used for local motion control of UAVs, but the UWB anchors were spaced tens of meters apart in the paper. In [15], a new UWB-based localization technique is proposed that can provide good localization accuracy in the case of relative motion between UAVs and ground vehicles and is suitable for UAV tracking and control in specific outdoor scenarios, but the performance of UAV localization in the landing phase is not described in the paper. In addition, the use of combined UWB and vision for landing was proposed in [16], where the authors deployed four UWB anchors around a 1.5m × 1m landing platform. The authors place a vision-located cooperative target on the landing platform, fuse UWB data with vision data and inertial data, and achieve a safe landing. However, the system must ensure that the cooperative target on the landing platform is within the camera's field of view, and the paper does not mention the performance of this system under poor light conditions. In addition, a localization optimization method is proposed in [17] to improve the localization accuracy and attitude accuracy by using the spacing of multiple tags as a constraint and filtering the redundant distances.

In response to the problems mentioned above regarding UAV localization during landing, this paper proposes a UAV localization system based on a landing platform, which combines data from two UWB tags and IMU to estimate the position of the UAV when it approaches or leaves the landing platform. In our localization system, similar to that described in [18], UWB anchors are placed on the four corners of the rectangular landing platform, and the UAV in this paper is equipped with two UWB tags and a six-axis IMU, where the IMU is the built-in IMU of the UAV. And our localization system has high localization accuracy and robustness. Our localization system is calculated in the UAV's onboard computer and works in two steps. In the first step, the two UWB tags carried by the UAV provide the measured distance from the anchor on the rectangular landing platform, and the initially calculated position of the two UWB tags is obtained. In the second step, the two UWB tags positions are fused with IMU data to obtain the final localization results. Compared to the schemes proposed by other researchers, our localization system does not depend on good lighting conditions and

GNSS usage environment, which means that it does not have high requirements for the environment. The configuration of two UWB tags improves localization accuracy, and the UWB anchors can be quickly deployed on top of the ground mobile landing platform.

The remaining content of this paper is organized as follows. Section II introduces the UWB localization principle and describes the steps for implementing our localization system. Section III explains and analyzes the experiments and evaluates the performance of our localization system by multiple experiments. Finally, in Section IV, conclusions are given, and the problems of our localization system and future research ideas are described.

II. SYSTEM ARCHITECTURE

A. UWB Localization System Principle

In a UWB-based real-time localization system, the UWB tag communicates with each UWB anchor to obtain the measured distance between the UWB tag and each UWB anchor, and the position of the UWB tag is uniquely determined by the measured distance constraint. Thus, the UWB tag localization problem can be described as follows: the distance between a point in the three-dimensional space and N position-determined points is known, then where is the position of the point? The precondition for solving this problem must ensure that $N \geq 4$. Assume that there exist four UWB anchors with known positions, $A_0 = [X_0 \ Y_0 \ Z_0]^T$, $A_1 = [X_1 \ Y_1 \ Z_1]^T$, $A_2 = [X_2 \ Y_2 \ Z_2]^T$, $A_3 = [X_3 \ Y_3 \ Z_3]^T$. According to the geometric constraints, the following set of equations can be listed.

$$\begin{cases} \tilde{d}_0 = \|A_0 - P\| + \varepsilon_0 \\ \tilde{d}_1 = \|A_1 - P\| + \varepsilon_1 \\ \tilde{d}_2 = \|A_2 - P\| + \varepsilon_2 \\ \tilde{d}_3 = \|A_3 - P\| + \varepsilon_3 \end{cases} \quad (1)$$

where \tilde{d}_k is the measured distance from the UWB tag to each UWB anchor, ε_k is the distance measurement error, $P = [x \ y \ z]^T$ is the UWB tag coordinate to be solved, and A_k is the coordinate of the UWB anchor k , $k = 0, 1, 2, 3$.

Equations (1) is a nonlinear system of equations about x , y , z . It is not easy to solve directly and may lead to no solution for (1) due to the presence of distance measurement error. Therefore, the above UWB tag localization problem is converted from a nonlinear system of equations exact solution problem to an optimal estimation problem of nonlinear optimization.

The optimal estimation problem of nonlinear optimization for tag localization has many methods to solve to obtain the coordinates of the tags, such as the linear least squares, the Gauss-Newton method, and the recently emerged bionic-optimization-based localization algorithms [19-23]. In the line-of-sight case, ε_k is usually modelled as a zero-mean Gaussian random variable[24]. For the linear least squares

method, it first transforms (1) into the following linear system of equations, where A_3 is chosen reference anchor point.

$$\begin{cases} DP = b \\ D = \begin{bmatrix} x_0 - x_3 & y_0 - y_3 & z_0 - z_3 \\ x_1 - x_3 & y_1 - y_3 & z_1 - z_3 \\ x_2 - x_3 & y_2 - y_3 & z_2 - z_3 \end{bmatrix} \\ b = \frac{1}{2} \begin{bmatrix} \tilde{d}_3^2 - \tilde{d}_0^2 + x_0^2 + y_0^2 + z_0^2 - x_3^2 - y_3^2 - z_3^2 \\ \tilde{d}_3^2 - \tilde{d}_1^2 + x_1^2 + y_1^2 + z_1^2 - x_3^2 - y_3^2 - z_3^2 \\ \tilde{d}_3^2 - \tilde{d}_2^2 + x_2^2 + y_2^2 + z_2^2 - x_3^2 - y_3^2 - z_3^2 \end{bmatrix} \end{cases} \quad (2)$$

The least squares solution of (2) is given by

$$P = (D^T D)^{-1} D^T b \quad (3)$$

In our UAV localization system based on a landing platform, the four UWB anchors lie in a horizontal plane, therefore the matrix D is singular. Thus, the linear least squares method is first used to obtain the coordinates x and y . The linear system of equations is

$$\begin{cases} UW = v \\ U = \begin{bmatrix} x_0 - x_3 & y_0 - y_3 \\ x_1 - x_3 & y_1 - y_3 \\ x_2 - x_3 & y_2 - y_3 \end{bmatrix} \\ v = \frac{1}{2} \begin{bmatrix} \tilde{d}_3^2 - \tilde{d}_0^2 + x_0^2 + y_0^2 - x_3^2 - y_3^2 \\ \tilde{d}_3^2 - \tilde{d}_1^2 + x_1^2 + y_1^2 - x_3^2 - y_3^2 \\ \tilde{d}_3^2 - \tilde{d}_2^2 + x_2^2 + y_2^2 - x_3^2 - y_3^2 \end{bmatrix} \end{cases} \quad (4)$$

The least squares solution is given by

$$W = (U^T U)^{-1} U^T v \quad (5)$$

where $W = (x, y)^T$.

B. UAV localization system based on a landing platform

Our UAV localization system based on a landing platform is designed for UAVs that perform large-range hazardous area detection tasks, such as nuclear power plants where accidents occur. In executing a large range of dangerous area detection tasks, the UAV has insufficient range and needs to land and recharge. If it returns to the take-off point to land and recharge, the range of UAV detectable area is too small, and the UAV may adhere to radioactive substances when executing tasks over the area where the nuclear accident occurred, and the UAV may cause harm to the surrounding personnel when it returns to the take-off point to land. Therefore, this paper proposes a UAV localization system based on a landing platform that can be conveniently deployed on an unmanned vehicle and powered by the power supply on the unmanned vehicle. The UAV can land on top of the landing platform carried by the unmanned vehicle according to the localization information provided by our localization system, and the UAV is transported to the next mission area and charged by the unmanned vehicle.

In our localization system, UWB and IMU data are fused to estimate the position of the UAV. Fig. 1 depicts the architecture and coordinate system of our localization system. Four UWB anchors are installed around the $0.8\text{m} \times 1.4\text{m}$

rectangular landing platform, and two UWB tags are installed on both sides of the UAV landing gear with a spacing of 0.39m . As shown in Fig. 1, in our localization system, the body coordinate system B is established with the center point of the UAV as the origin, the nose of the UAV as the positive X -axis direction, the left side as the positive Y -axis direction, and the upward as the positive Z -axis direction. All IMU measurements are referenced to the body coordinate system B . The right-handed inertial coordinate system A is established with the position of anchor 0 on the landing platform as the origin, and the coordinate system A is fixed to the landing platform.

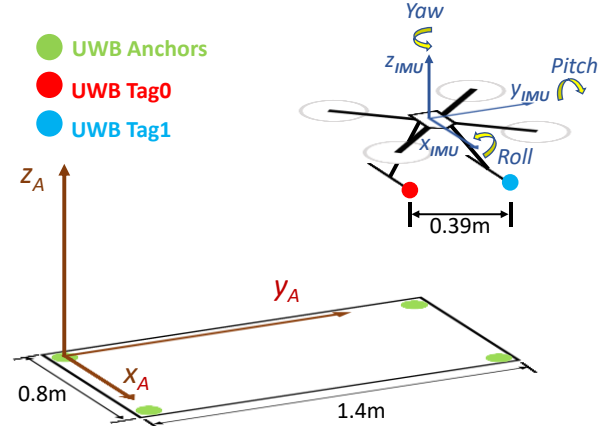


Fig. 1. The architecture and coordinate system of the UAV localization system based on a landing platform.



Fig. 2. DJI M300RTK and UWB tag installation position on the UAV.

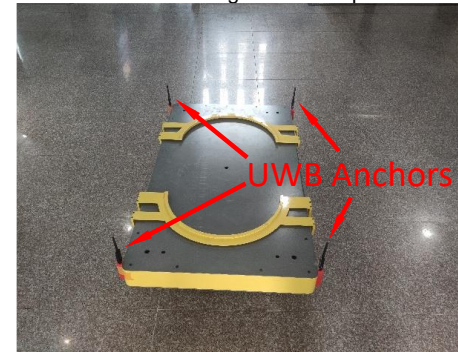


Fig. 3. The landing platform.

In terms of localization algorithms, although the linear least squares method is simple and widely used, the coordinate calculated by the linear least squares of the tag is not very accurate due to error in ranging performed by the UWB tag and when the geometric configuration of the four anchor deployments is poor [25]. Thus, we install two tags on the UAV and propose an algorithm that adds the ranging

information between the two tags and each anchor and the spacing between the two tags to the localization algorithm to calculate the position of UWB tags and then fuse it with the IMU data to obtain an estimate of the position of the center of the UAV. In fact, in the end, it is only necessary to use the coordinates of the horizontal direction of the UAV, because the height (i.e. distance to the ground) can be estimated using onboard sensors such as the altimeter.

Table I describes the information of the UWB module installed on the landing platform and UAV, including chip, carrier frequency, range, bitrate, transmit power, channel bandwidths, power consumption, size of the module, and precision. Fig. 2 shows the DJI M300RTK UAV used and the position of the two UWB tags installed on the UAV. IMU data used for our localization system are provided by the UAV's built-in IMU. Fig. 3 shows the landing platform used for our localization system.

TABLE I

THE INFORMATION OF UWB MODULE [26]

Parameter	Value	Units
Chip	DW1000	-
Carrier frequency	3.2-6.9	GHz
Range	100	m
Bitrate	6.8	Mbps
Transmit power	-35 - -62	dbm/MHz
Channel bandwidths	500	MHz
Power consumption	0.528	W
Size of module	84×25×12	mm
Precision	<10	cm

Fig. 4 depicts the workflow of our localization system. The workflow of our localization system mainly consists of two parts: the Two-tags-based UWB localization optimization algorithm and the Kalman-filter-based UWB and IMU localization fusion algorithm. Firstly, the UWB tag communicates with the UWB anchor by using the two-way ranging method, and the UWB tag calculates the distance to each UWB anchor. r_{0j} and r_{1j} represent the raw measured range between UWB tag 0 and UWB tag 1 and the anchor j , respectively. Then the raw range is Kalman filtered to obtain the filter range r_{0j}^f and r_{1j}^f . And the system covariance Q of the 1D Kalman filter is 0.018, and the observation covariance R of the 1D Kalman filter is 0.542. The initial 2D plane coordinates $W_0 = (x_0, y_0)^T$ and $W_1 = (x_1, y_1)^T$ of the two UWB tags are calculated by using the linear least squares. The height h of the UAV is used as the coordinates in the z-direction to obtain the initial coordinates $P_0 = [W_0^T \ h]^T$ and $P_1 = [W_1^T \ h]^T$.

Subsequently, P_0 , P_1 , and the distance l of the two UWB tags are substituted into the predefined cost function J , and the positions of the two UWB tags are obtained using the gradient descent method. Finally, the coordinates of the two UWB tags are summed and averaged to obtain the position of the center of the two UWB tags P'_C . P'_C is fused with the IMU data as the input to the Kalman filter to obtain the final localization result P_C^f .

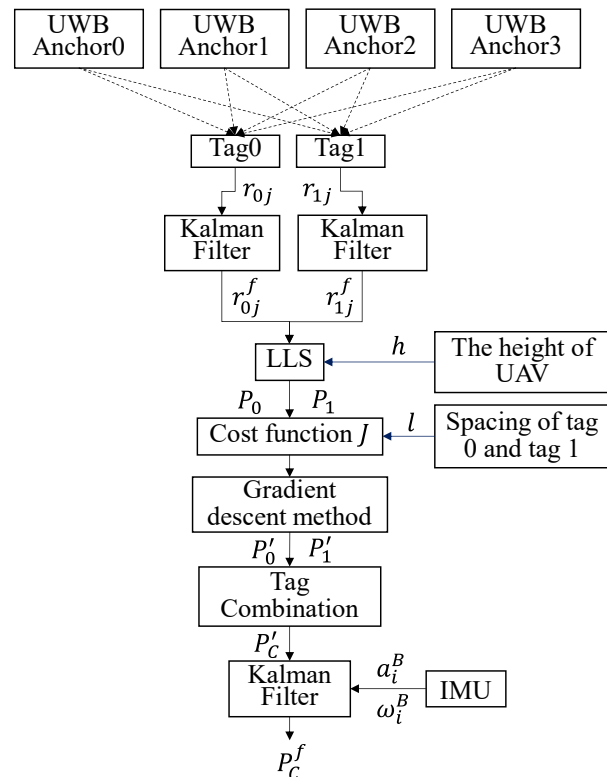


Fig. 4. Workflow of the UAV localization system based on a landing platform. LLS represents the linear least squares.

C. Two-tags-based UWB localization optimization algorithm

In UWB-based localization systems, as mentioned in Section II-B, the linear least squares is easy to calculate and widely used, but the optimization objective function of linear least squares is

$$\begin{aligned}
 P &= \min_P \|DP - b\|^2 \\
 &= \min_P \sum_{k=1,2,3} \left[\|P - A_k\|^2 - \tilde{d}_k^2 - \left(\|P - A_0\|^2 - \tilde{d}_0^2 \right) \right]^2 \quad (6)
 \end{aligned}$$

In some cases, the results obtained by the linear least squares method produce huge errors [27] and can make (1) ill-conditioned when the localization geometry configuration is poor, leading to unreliable localization results [25]. Although deployment with UWB anchors spaced 2 m apart is suggested in [13], this deployment scheme still has the problem of too large a deployment area for unmanned vehicles. Therefore, in our localization system, the two-tags-based UWB localization optimization algorithm is used, where four UWB anchors are deployed at the four corners of a $0.8\text{m} \times 1.4\text{m}$ rectangle, and two UWB tags are installed on the UAV to add redundant distance constraints to reduce the error in UAV position estimation. As shown in Fig. 5, the algorithm first solves the initial coordinates of the two UWB tags P_0 and P_1 using the linear least squares method, where the z-direction coordinate of P_0 and P_1 is the height h of the UAV. And then the initial coordinates of the two UWB tags and the distance l of the two UWB tags are substituted into the cost function J . The localization coordinates P_0' and P_1' of the two UWB tags are solved using the gradient descent method.

Firstly, define the cost function J .

$$J = 200 \left(\|P_0 - P_1\|^2 - l^2 \right)^2 + \sum_{m,n} \left(\|P_m - A_n\|^2 - d_{mn}^2 \right)^2 \quad (7)$$

where P_0 is the coordinate of UWB tag 0, P_1 is the coordinate of UWB tag 1, l is the distance between two UWB tags, P_m is the coordinate of the UWB tag m , $m \in \{0,1\}$, A_n is the coordinate of UWB anchor n , $n \in \{0,1,2,3\}$, and d_{mn} is the measured distance between the UWB tag m and the UWB anchor n . Since l is fixed and is measured using a metal tape measure with high accuracy, the factor 200 is set in the cost function J .

Subsequently, the partial derivatives of the cost function J concerning the two UWB tags coordinates are calculated separately.

$$\frac{\partial J}{\partial P_m} = (-1)^m 800 \left(\|P_0 - P_1\|^2 - l^2 \right) (P_0 - P_1)^T + \sum_n 4 \left(\|P_m - A_n\|^2 - d_{mn}^2 \right) (P_m - A_n)^T \quad (8)$$

Then the number of iterations λ is limited. When the number of iterations $\lambda > 100$, stops the iterative solution and output the localization coordinates P_0^i and P_1^i of the two UWB tags at this time. If $\lambda \leq 100$, judge the convergence condition: $|J_t - J_{t-1}| < \zeta$, $\zeta = 0.001$. If the condition is not satisfied, then

$$P_m = P_m - \Delta \frac{\partial J}{\partial P_m} \quad (9)$$

where $\Delta = 0.001$ is the iteration step size. Then continue calculating the cost function, judging the convergence condition, and finally get the localization coordinates P_0^i and P_1^i of the two UWB tags.

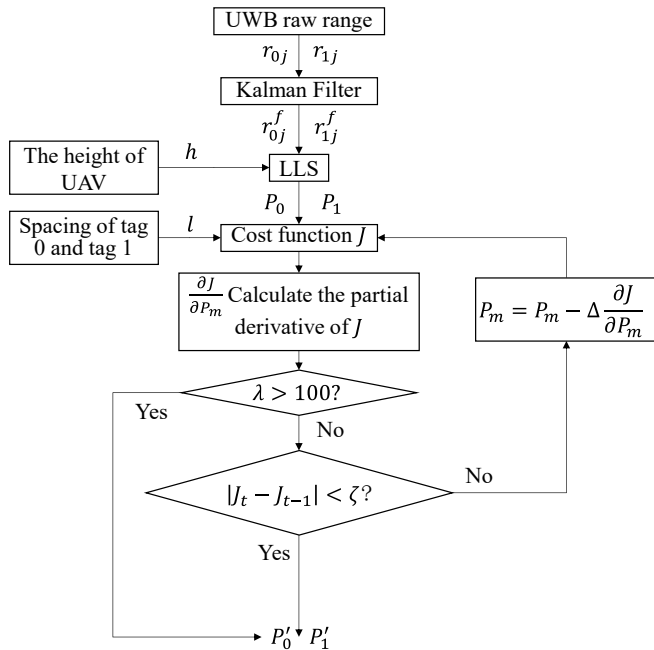


Fig. 5. Workflow of Two-tags-based UWB localization optimization algorithm. LLS represents the linear least squares.

D. Kalman-filter-based UWB and IMU localization fusion algorithm

The workflow of the Kalman-filter-based UWB and IMU localization fusion algorithm is shown in Fig. 6. After obtaining the position coordinate of the two UWB tags using our Two-tags-based UWB localization optimization algorithm, the coordinates of the two tags are summed and averaged to obtain the coordinate P_C^i of the middle position of the two tags. Then the accelerometer and gyroscope data are read from the IMU and used with P_C^i as the input of the Kalman filter to obtain the final localization result P_C^f .

Due to the different rates of IMU and UWB, time synchronization is required when fusing the two data. The localization frequency of two UWB tags using our Two-tags-based UWB localization optimization algorithm is 20Hz, whereas the frequency of IMU carried by UAV is up to 400Hz, so it is necessary to downsample IMU to realize the time synchronization. Among the IMU data, the accelerometer and gyroscope data are referenced to the body coordinate system B , which needs to be converted to the landing platform coordinate system A , i.e.

$$a_i^A = R_B^A a_i^B \quad (10)$$

$$\omega_i^A = R_B^A \omega_i^B \quad (11)$$

where a_i^B denotes the acceleration of the UAV under coordinate system B at the time i , a_i^A denotes the acceleration of the UAV under coordinate system A at the time i , ω_i^B denotes the angular velocity of the UAV under coordinate system B at the time i , ω_i^A denotes the angular velocity of the UAV under coordinate system A at the time i , and R_B^A denotes the rotation matrix when rotating from the body coordinate system B to coordinate system A .

Before fusing IMU data with UWB localization data, the initial attitude of the UAV needs to be obtained, so the UAV is parked for a period of time, and the current roll angle ϕ and pitch angle θ are obtained by the condition that the UAV is subjected to gravity only, and let the yaw angle ψ be 0. Assume that the acceleration of gravity in the coordinate system B is $G = [0 \ 0 \ -g]^T$, and the accelerometer data in the parked state is $a_i^B = [a_x \ a_y \ a_z]^T$, then we have $G = R_B^A a_i^B$.

$$R_B^A = \begin{bmatrix} c\theta c\psi & c\psi s\theta s\phi - c\phi s\psi & s\phi s\psi + c\phi c\psi s\theta \\ c\theta s\psi & c\phi c\psi + s\theta s\phi s\psi & c\phi s\theta s\psi - s\phi c\psi \\ -s\theta & c\theta s\phi & c\theta c\phi \end{bmatrix} \quad (12)$$

where $c\theta = \cos\theta$, $s\theta = \sin\theta$, $c\psi = \cos\psi$, $s\psi = \sin\psi$, $s\phi = \sin\phi$, $c\phi = \cos\phi$.

Solving $G = R_B^A a_i^B$ yields the roll angle $\phi = \arctan(a_y, a_z)$ and the pitch angle $\theta = \arcsin\left(a_x \sqrt{a_x^2 + a_y^2 + a_z^2}\right)$. After obtaining the attitude of the UAV through initialization,

complementary filtering [28] is used to update the attitude angle of the UAV and further update the rotation matrix R_B^A of the body coordinate system B and the landing platform coordinate system A .

In the Kalman-filter-based UWB and IMU localization fusion algorithm, the state vectors include position, velocity, and acceleration.

$$x_i = \begin{bmatrix} p_i^T & v_i^T & (a_i^A)^T \end{bmatrix}^T \quad (13)$$

where p_i , v_i , and a_i^A are the position, velocity, and acceleration of the UAV at the time i in the coordinate system A .

Define the following equations of state and observation equations.

$$x_i^- = Fx_{i-1} \quad (14)$$

$$y_i^- = Hx_i^- \quad (15)$$

where x_{i-1} is the state vector at time $i-1$, x_i^- is the a priori state vector, and y_i^- is the a priori observation vector predicted from the a priori state vector x_i^- . F is the state transfer matrix, and the expression is

$$F = \begin{bmatrix} I & Idt & \frac{1}{2}Idt^2 \\ O & I & Idt \\ O & O & I \end{bmatrix} \quad (16)$$

where I is the 3×3 identity matrix, dt is the sampling period, and O is the null matrix.

H in (15) is the observation matrix, and the expression is

$$H = \begin{bmatrix} I & O & O \\ O & I & O \\ O & O & I \end{bmatrix} \quad (17)$$

The priori covariance matrix is

$$E_i^- = FE_{i-1}F^T + Q \quad (18)$$

where E_{i-1} is the posterior covariance matrix at time $i-1$ and Q is the process noise covariance matrix.

The Kalman gain is

$$K_i = E_i^- H^T [(HE_i^- H^T) + R]^{-1} \quad (19)$$

where R is the measurement noise covariance matrix.

The observation vector y_i consists of the coordinate P_C of the middle of the two tags and the acceleration a_i^A .

$$y_i = \begin{bmatrix} (P_C)^T & O & (a_i^A)^T \end{bmatrix}^T \quad (20)$$

Finally, the priori observation vector y_i^- is compared with the sensor's observation vector y_i to obtain the residuals, and then the prior state vector x_i^- is corrected to obtain the a posteriori optimal estimate of the state vector, i.e.

$$x_i = x_i^- + K_i (y_i - y_i^-) \quad (21)$$

According to K_i , the posterior covariance matrix at time i can be calculated as

$$E_i = (I - K_i H) E_i^- \quad (22)$$

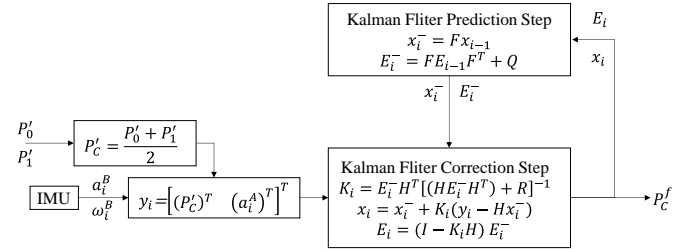


Fig. 6. Workflow of Kalman-filter-based UWB and IMU localization fusion algorithm.

III. EXPERIMENT AND ANALYSIS

In order to evaluate our localization system, we conducted indoor static localization experiments and outdoor flight experiments, respectively. All experiments were conducted on the UAV with an onboard computer. The onboard computer is a Manifold 2G manufactured by DJI running Ubuntu 16.04 with an NVIDIA Jetson TX2 processor. And the UAV is the M300RTK UAV produced by DJI. UWB tags are connected to the onboard computer through the USB serial port, and the onboard computer communicates with the UAV to acquire IMU data through the Onboard SDK adapter board produced by DJI. The experiment setup is shown in Fig. 7. Several positions were selected for indoor static localization experiments to evaluate our Two-tags-based UWB localization optimization algorithm. We conducted several outdoor flight experiments to evaluate our UAV localization system based on a landing platform.

The workflow of our localization system is depicted in Fig. 4. After the two UWB tags obtain the measured distance from the UWB anchors, the initial coordinates P_0 and P_1 are obtained by merging the initial coordinates x and y calculated by the least squares method and the height h of the UAV. P_0 , P_1 , and l are substituted into the cost function J . Then P_0' and P_1' obtained by the gradient descent method and the IMU data are fused by the Kalman filter to obtain the final localization result.

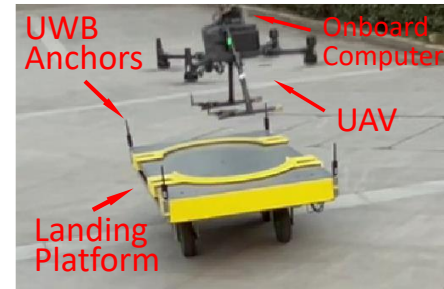


Fig. 7. The experiment setup.

A. Static localization experiment

We firstly conducted static localization experiments indoors to evaluate our Two-tags-based UWB localization optimization algorithm. The experimental environment is shown in Fig. 8. All static localization experiments were conducted indoors, and the real coordinates of the test points were measured by a metal tape measure, and the coordinates of each UWB anchor are shown in Table II. The linear least squares method is one of the commonly used tag localization

methods, and the linear least squares method is chosen for comparison in this paper.



Fig. 8. Static localization experimental environment.

TABLE II
UWB ANCHOR COORDINATES

Anchors	x(m)	y(m)	z(m)
A0	0	0	0
A1	0	1.4	0
A2	-0.8	1.4	0
A3	-0.8	0	0

TABLE III
RMSE AND AVERAGE NUMBER OF ITERATIONS

Experiment t	UW B tag	True coordinate	RMSE of linear least squares	RMSE of our localization optimization algorithm	Average number of iterations
1	0	(0.73,0,0)	0.158	0.073	39.3
	1	(0.73,0.39,0)	0.149	0.075	
2	0	(1.76,0,0)	0.221	0.107	24.5
	1	(1.76,0.39,0)	0.278	0.110	
3	0	(0.42,0.7,0)	0.164	0.089	56.7
	1	(0.42,0.31,0)	0.130	0.089	
4	0	(0,0.81,0)	0.109	0.037	53.7
	1	(0,0.42,0)	0.050	0.033	
5	0	(-0.25,0.65,0)	0.082	0.051	29.0
	1	(-0.25,1.04,0)	0.169	0.093	
6	0	(0.2,31,0)	0.329	0.279	21.1
	1	(-0.39,2.31,0)	0.229	0.139	

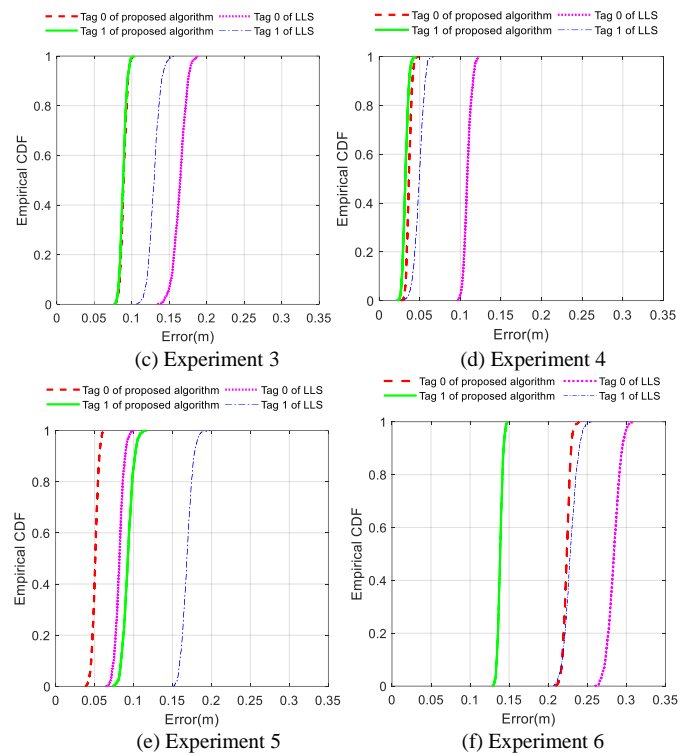
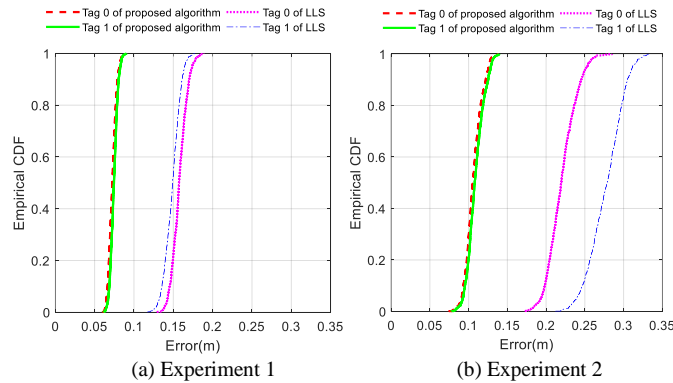


Fig. 9. Cumulative distribution function plots of each UWB tag using our proposed Two-tags-based UWB localization optimization algorithm and the linear least squares method in 6 experiments. The proposed algorithm is the Two-tags-based UWB localization optimization algorithm and LLS is the linear least squares.

Table III gives the true coordinates of the two UWB tags, the root mean square error (RMSE), and the average number of iterations using different solution methods for all the static localization experiments, which consisted of 6 experiments with 720 data samples per set. Fig. 9 depicts the cumulative distribution of localization error for UWB tags with different localization algorithms in 6 sets of experiments. The red dashed line shows the cumulative distribution of localization error for UWB tag 0 using our Two-tags-based UWB localization optimization algorithm. The green solid line shows the cumulative distribution of localization error for UWB tag 1 using our Two-tags-based UWB localization optimization algorithm. The magenta dotted line shows the cumulative distribution of locating error for UWB tag 0 using the linear least squares method, and the blue dash-dotted line shows the cumulative distribution of locating error for UWB tag 1 using the linear least squares method. The root-mean-square error obtained by using our Two-tags-based UWB localization optimization algorithm is significantly lower than that of the linear least squares method, and the localization error of the UWB localization algorithm is more stable.

In addition, the average number of iterations in the 6 groups of experiments all of them are below 60. In Experiment 3, Experiment 4, Experiment 5, and Experiment 6, the average computation time of our Two-tags-based UWB localization optimization algorithm for each localization in the three sets of experiments was 18.24ms in Experiment 3, 18.98ms in Experiment 4, 13.22ms in Experiment 5, and 5.83ms in Experiment 6. Thus, our Two-tags-based UWB localization optimization algorithm has good real-time performance and meets the real-time localization requirements.

B. Flight Localization Experiment

In order to evaluate our localization system, several flight experiments were conducted, all of which were outdoors. To track the UAV with centimeter-level accuracy, RTK localization data on the M300 RTK UAV were used as the ground truth, and the UAV network RTK differential data were provided by QianXun Location Network Co. with a position accuracy of 1 cm+1ppm. The UAV experimental environment is shown in Fig. 10, and the coordinates of each UWB anchor are consistent with those shown in Table II. The coordinate system of RTK localization data is not consistent with that of our localization system, and in order to compare the RTK localization data with our localization system, the RTK localization data need to be converted. Firstly, the latitude and longitude coordinates of each UWB anchor are measured using RTK, and then the planar projection coordinates are obtained using Gauss-Krüger projection. There is a rotation translation relationship between the plane projection coordinate system and the coordinate system of our localization system. The rotation and translation matrices can be solved by the one-to-one correspondence between the plane projection coordinates of each UWB anchor and the coordinates of each UWB anchor in Table II. The singular value decomposition method is one of the very excellent methods for solving such problems. Thus, this method is chosen to solve the rotation and translation matrices of the plane projection coordinate system and the coordinate system of our localization system [29].



Fig. 10. Flight localization experiment environment.

The results of the flight experiments are shown in Fig. 11 and Table IV, which include five experiments. The green trajectory in Fig. 11 is the localization trajectory of our

localization system. As a comparison, the initial coordinate of one of the two UWB tags installed on the UAV is solved using linear least squares, and this initial coordinate and the IMU data are subsequently fused as inputs to the Kalman filter, and this method is named the single-tag method in the following. The red localization trajectory in Fig. 11 is the localization trajectory of the single-tag method. The black trajectory is the RTK localization trajectory as the ground truth in the experiment. The blue line represents the landing platform. Table IV shows the main statistics for each flight experiment in Fig. 11, including RMSE, error mean μ , standard deviation σ , and maximum error.

The experimental results show that the maximum root mean square error is 0.6875m, and the minimum is 0.1813m in 5 experiments for the single-tag method. As mentioned in Section II-B, the linear least squares method leads to huge error in some specific cases, and the poor localization configuration in the flight experiments tends to make (1) ill-conditioned, which leads to the experimental results presenting large error and error fluctuations. In contrast, the root mean square error of our localization system is 0.2164m, 0.2303m, 0.1882m, 0.1071m, and 0.092m in five groups of experiments, with the maximum root mean square error of 0.2303m and the minimum root mean square error of 0.092m. Compared with the single-tag method, the RMSE of our localization system was reduced by an average of 61%. The error fluctuation of the localization results is not large and more stable, the root mean square error is small, and the localization results are reliable.

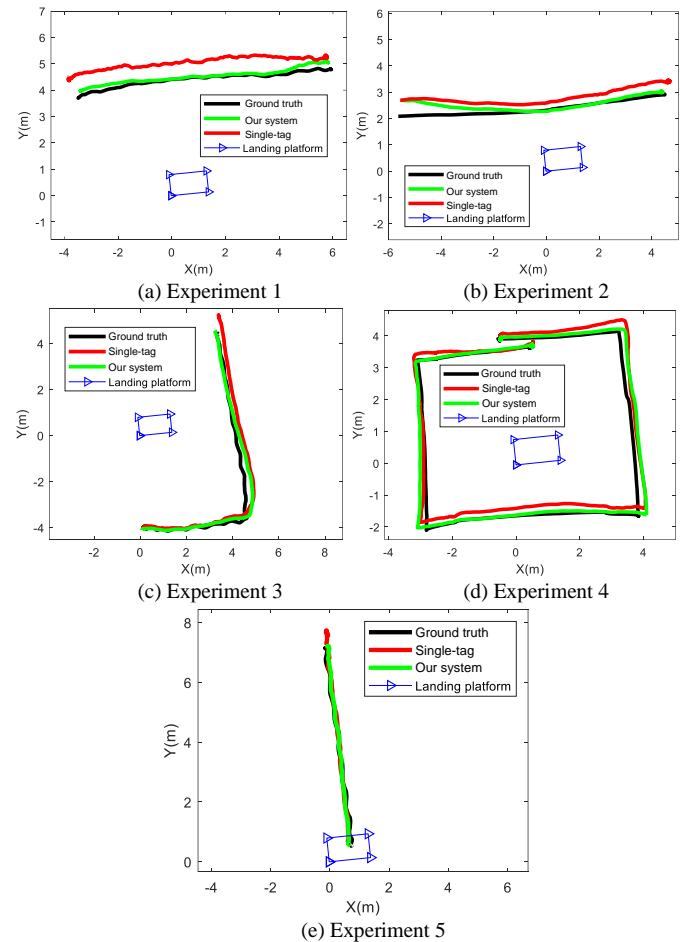


TABLE IV

THE MAIN STATISTICS OF ALL FLIGHT EXPERIMENTS USING THE SINGLE-TAG METHOD AND OUR SYSTEM.

Experiment	Method	RMSE	μ	σ	Max error
Experiment1	Single-tag	0.688	0.6769	0.1202	0.867
	Our system	0.216	0.1989	0.0860	0.406
Experiment2	Single-tag	0.463	0.4467	0.1215	0.753
	Our system	0.230	0.1919	0.1276	0.621
Experiment3	Single-tag	0.305	0.2598	0.1602	0.819
	Our system	0.188	0.1706	0.0795	0.328
Experiment4	Single-tag	0.181	0.1612	0.0832	0.384
	Our system	0.107	0.0769	0.0769	0.301
Experiment5	Single-tag	0.494	0.4371	0.2309	0.914
	Our system	0.092	0.0852	0.0347	0.168

Fig. 11. Flight experiments trajectory. The green solid line is the flight localization trajectory of our UAV localization system based on a landing platform. The red solid line is the flight localization trajectory of the single-tag method. The black solid line is the ground truth of the flight trajectory. The blue triangle solid line is the landing platform area.

In the five groups of experiments, the localization results of our localization system have significantly improved the localization accuracy compared with the localization results of the single-tag method. In experiment 1, experiment 2, experiment 3, and experiment 4, although the error of our localization system is reduced compared with the single-tag method, the localization error increases significantly when the UAV is far away from the landing platform and asymmetric concerning the four UWB anchors in both the X -axis and Y -axis directions, such as at the X -axis coordinate of -5m in experiment 2, which is due to the poor localization configuration in these specific areas, leading to the localization accuracy significantly decreased. However, when the UAV gradually approaches the landing platform, such as near the X -axis coordinate of 0m in experiment 2, the localization accuracy of our localization system improves significantly, so the significant increase of error in some areas shown in the experiments does not affect the UAV's approach to the landing platform for landing.

In addition, our localization system pays more attention to the localization performance in the UAV approach phase. Experiment 5 in Fig. 11 shows the localization performance in the case of the UAV approaching the platform, and the root mean square error of our localization system is described in Table IV as 0.092m in Experiment 5, which meets the localization demand of UAV landing in the landing platform.

IV. CONCLUSION

This paper proposes a UAV localization system based on a landing platform, which contains four UWB anchors placed on the landing platform and two tags and IMUs installed on the UAV. And the UAV localization system based on a landing platform can provide more accurate localization for the UAV when the UAV lands. Unlike the classical visual localization system, our UAV localization system based on a landing platform is not affected by light conditions such as smoke and does not depend on GPS, and the area occupied by the anchor deployment is small, which can be conveniently deployed on an unmanned vehicle.

Our UAV localization system based on a landing platform is different from the traditional UWB real-time localization system in that it defines a cost function that fuses the distance between two UWB tags and the ranging data of two UWB tags, solves the cost function using the gradient descent method to obtain the coordinates of two UWB tags, and uses Kalman filtering to fuse with IMU to obtain the final localization coordinates. The experimental results show that our localization system can provide decimeter-level localization accuracy for the UAV landing on the landing platform, and the average RMSE of our proposed localization system is reduced by 61% compared with the traditional single-tag method. However, our proposed localization system does not fully use of the two UWB tags localization data to provide directional information for the UAV and relies on the altitude data provided by the UAV. In future research, we will consider

installing three UWB tags on the UAV and fusing them with the IMU to provide good attitude and localization information for the UAV.

REFERENCES

- [1] A. Gautam, P. B. Sujit and S. Saripalli, "A survey of autonomous landing techniques for UAVs," *2014 International Conference on Unmanned Aircraft Systems (ICUAS)*, 2014, pp. 1210-1218, doi: 10.1109/ICUAS.2014.6842377.
- [2] X. Liu *et al.*, "Challenges and Opportunities for Autonomous Micro-UAVs in Precision Agriculture," in *IEEE Micro*, vol. 42, no. 1, pp. 61-68, 1 Jan.-Feb. 2022, doi: 10.1109/MM.2021.3134744.
- [3] D. Yulong, Bin Xin, and Jie Chen. "A review of recent advances in coordination between unmanned aerial and ground vehicles," *Unmanned Systems*, vol. 09, no.02, Aug. 2021.
- [4] A. Aboumrad, J. Haun, A. McGinnis and N. Wu, "An Automatic Platform for Landing and Charging of UAVs to Extend UAV Operations," *2020 16th International Conference on Distributed Computing in Sensor Systems (DCOSS)*, 2020, pp. 343-347, doi: 10.1109/DCOSS49796.2020.00061.
- [5] Q. Vu *et al.* "Trends in development of UAV-UGV cooperation approaches in precision agriculture," *International Conference on Interactive Collaborative Robotics*. Springer, Cham, 2018, pp. 213-221.
- [6] U. Hakan, U. Yuzgec, and C. Bayilmis. "A review on applications of rotary-wing unmanned aerial vehicle charging stations," *International Journal of Advanced Robotic Systems*, vol. 18, no.3, May 2021.
- [7] N. A. Elmunim and M. Abdullah, "Overview of the GPS," *Ionospheric Delay Investigation and Forecasting*. Springer, Singapore, 2021. 5-17.
- [8] F. Liu, H. Han, X. Cheng, and B. Li, "Performance of Tightly Coupled Integration of GPS/BDS/MEMS-INS/Odometer for Real-Time High-Precision Vehicle Positioning in Urban Degraded and Denied Environment," *Journal of Sensors*, vol. 2020, 2020.
- [9] S. Saripalli, J.F. Montgomery, and G.S. Sukhatme, "Visually guided landing of an unmanned aerial vehicle," *IEEE transactions on robotics and automation* vol. 19, no.3, pp. 371-380, Jun. 2003.
- [10] C. Chang *et al.*, "Proactive Guidance for Accurate UAV Landing on a Dynamic Platform: A Visual-Inertial Approach," *Sensors*, vol. 22, no. 1, 2022.
- [11] P.H. Nguyen *et al.* "LightDenseYOLO: A fast and accurate marker tracker for autonomous UAV landing by visible light camera sensor on drone," *Sensors*, vol. 18, no. 6, 2018.
- [12] Y. ZHAO *et al.* "Dynamic tracking and precise landing of UAV based on visual magnetic guidance," *Journal of ZheJiang University (Engineering Science)*, vol. 55, no. 1, pp. 96-108, 2021.
- [13] J. P. Queralt, C. Martínez Almansa, F. Schiano, D. Floreano and T. Westerlund, "UWB-based System for UAV Localization in GNSS-Denied Environments: Characterization and Dataset," *2020 IEEE/RSJ International Conference on Intelligent Robots and Systems (IROS)*, 2020, pp. 4521-4528, doi: 10.1109/IROS45743.2020.9341042.
- [14] K. Cisek, A. Zolich, K. Klausen and T. A. Johansen, "Ultra-wide band Real time Location Systems: Practical implementation and UAV performance evaluation," *2017 Workshop on Research, Education and Development of Unmanned Aerial Systems (RED-UAS)*, 2017, pp. 204-209, doi: 10.1109/RED-UAS.2017.8101667.
- [15] F. Lazzari, A. Buffi, P. Nepa and S. Lazzari, "Numerical Investigation of an UWB Localization Technique for Unmanned Aerial Vehicles in Outdoor Scenarios," *IEEE Sensors Journal*, vol. 17, no. 9, pp. 2896-2903, May 2017.
- [16] T. H. Nguyen, M. Cao, T. -M. Nguyen and L. Xie, "Post-Mission Autonomous Return and Precision Landing of UAV," *2018 15th International Conference on Control, Automation, Robotics and Vision (ICARCV)*, 2018, pp. 1747-1752, doi: 10.1109/ICARCV.2018.8581117.
- [17] S. ZHANG *et al.* "UWB positioning optimization method based on redundant distance screening," *Journal of Tsinghua University (Science and Technology)*, vol. 62, no. 5, pp. 934-942, 2022.
- [18] T. -M. Nguyen, T. H. Nguyen, M. Cao, Z. Qiu and L. Xie, "Integrated UWB-Vision Approach for Autonomous Docking of UAVs in GPS-denied Environments," *2019 International Conference on Robotics and Automation (ICRA)*, 2019, pp. 9603-9609, doi: 10.1109/ICRA.2019.8793851.
- [19] X. Lou and Y. Zhao, "High-Accuracy Positioning Algorithm Based on UWB," *2019 International Conference on Artificial Intelligence and*

Advanced Manufacturing (AIAM), 2019, pp. 71-75, doi: 10.1109/AIAM48774.2019.00021.

- [20] C. Wang *et al.* "Bias analysis of parameter estimator based on Gauss-Newton method applied to ultra-wideband positioning," *Applied Sciences*, vol. 10, no. 1, 2019.
- [21] M. Ridolfi *et al.* "Self-calibration and Collaborative Localization for UWB Positioning Systems: A Survey and Future Research Directions," *ACM Computing Surveys*, vol. 54, no. 4, 2021.
- [22] X. Chen *et al.* "Harris hawks optimization algorithm and BP neural network for ultra-wideband indoor positioning," *Mathematical Biosciences and Engineering*, vol. 19, no. 9, pp. 9098-9124, 2022.
- [23] X. Cai, L. Ye, and Q. Zhang, "Ensemble learning particle swarm optimization for real-time UWB indoor localization," *EURASIP Journal on Wireless Communications and Networking*, vol. 2018, no.1, 2018.
- [24] C. Wang, "Study on UWB Positioning Method and Configuration Optimization," Ph.D. dissertation, Sch. Environ. Spatial Info., China Univ. of Mining and Technology, Xuzhou, China, 2020.
- [25] C. Wang *et al.* "Performance Analysis of Parameter Estimator Based on Closed-Form Newton Method for Ultrawideband Positioning," *Mathematical Problems in Engineering*, vol. 2020, 2020.
- [26] DW1000 Datasheet, Mouser Electronics, Inc., Delaware, USA, 2016. [Online]. Available: https://www.mouser.it/datasheet/2/412/DW1000_Datasheet-1878664.pdf
- [27] X. P. Wang, J. Luo, and C. X. Shen. "Research on the Stability of Trilateration Algorithms," *Computer Engineering & Science*, vol. 34, no. 6, pp. 12-17, 2012.
- [28] H. . -Q. . -T. Ngo, T. . -P. Nguyen, V. . -N. . -S. Huynh, T. . -S. Le and C. . -T. Nguyen, "Experimental comparison of Complementary filter and Kalman filter design for low-cost sensor in quadcopter," *2017 International Conference on System Science and Engineering (ICSSE)*, 2017, pp. 488-493, doi: 10.1109/ICSSE.2017.8030922.
- [29] O. Sorkine. "Least-Squares Rigid Motion Using SVD," *Technical notes*, vol. 120, no. 3, 2009.



Xia You received the M.S. degree in measurement and control technology and instrument from Nanjing University of Aeronautics and Astronautics in 2004. She is currently an associate researcher with the College of Automation Engineering, Nanjing University of Aeronautics and Astronautics, China. Her research interests include positioning and navigation of unmanned ground vehicles, and new energy power generation technology.



Qingxi Zeng received the B.S. degree in electrical engineering and automation from the Harbin Institute of Technology, Harbin, China, in 2002, and the Ph.D. degree in instrument science and technology from Southeast University, Nanjing, China, in 2009. In 2018, he was a Visiting Scholar with The Robotics Institute, Carnegie Mellon University, USA. He is currently an Associate Professor with the College of Automation Engineering, Nanjing University of Aeronautics and Astronautics, China. His research interests include positioning and navigation of unmanned ground vehicles, multi-sensor fusion systems, and GNSS software receiver.



Yu Jin was born in Jiangxi, China, in 1998. He received the B.S. degree from the Nanchang Hangkong University, China, in 2020. He is currently pursuing the M.S. degree with the College of Automation Engineering, Nanjing University of Aeronautics and Astronautics. His research interest includes robot navigation and positioning.



Haonan Yu was born in Jiangsu Province, China in 1999. He received his B.S. degree from the Yangzhou University, China in 2021. He is currently a M.S. student at the College of Automation Engineering, Nanjing University of Aeronautics and Astronautics. His research interest includes SLAM and robot vision.